Three-Dimensional Numerical Investigation on the Effect of Injector Configuration in Rotating Detonation Engine

Takumi Sada[1], Akiko Matsuo[1], Eiji Shima[1],
Hiroaki Watanabe[2], Akira Kawasaki[2], Ken Matsuoka[2], Jiro Kasahara[2]

[1]Department of Mechanical Engineering, Keio University
Hiyoshi, Kohoku-ku, Yokohama, Kanagawa, Japan

[2]Department of Aerospace Engineering, Nagoya University
Furo-cho, Chikusa-ku, Nagoya, Aichi, Japan

1 Introduction

Rotating detonation engine (RDE), which generates thrust by supersonic combustion, has been getting attention as a novel heat engine. Detonation in this engine can provide high theoretical thermal efficiency [1,2] and is expected to reduce the size of the combustor due to the compression effect by the shock wave and the rapid completion of combustion. So, the application of detonation to heat engines has been considered and there are a lot of research about it. In the typical RDE, detonation propagates through the unburned gas flowed from the bottom of the annular combustor. The expansion after the combustion accelerates the burned gas in the axial direction, and it is exhausted from the combustor outlet.

One of the problems for the practical use of RDE is the high heat load on the combustor walls because of the high temperature by the continuous propagation of detonation [3,4]. To achieve a long-time operation with a simple geometry, which is one of the advantages of detonation engines, the system is necessary that can cool the walls without using an external cooling system. To reduce this heat load on the combustor walls, Goto et al. [5] conducted an experiment using combustor with different structure than conventional RDEs. The features of this combustor are as follows. Firstly, the inner wall of the combustor is removed. Such a RDE, which is called a cylindrical or hollow RDE, can reduce the heat wall on the inner wall. It has been experimentally confirmed that it provides the similar performance as the annular RDE [6]. Numerical analysis has also shown that detonation propagation can be sustained in this geometry [7]. In addition, to reduce the heat load on the outer wall, the fuel and oxidizer are injected from the combustor side wall, as opposed to the conventional flow from the bottom expecting that the unburned gas would have a cooling effect. This experiment showed that the increase in heat flux

Correspondence to: t.sada000@keio.jp

to the wall was limited to about 18-25 % when the mass flow rate was doubled, and that a layer of unburned gas reduced the heat input near the outer wall of the combustor.

As described above, research has been conducted with injection from the combustor side wall to reduce the heat load. However, due to the propagation velocity of detonation and the complex flow field in RDE, it is difficult to observe the phenomena in detail, so the effect of the injector on the combustor side wall on the detonation propagation is not clear. So, the objective of this study is to clarify the effect of injector configuration on the detonation propagation in the cylindrical rotating detonation combustor. In this paper, an inviscid numerical analysis is performed with H_2-Air premixed gas injection for cylindrical RDE with a short combustor used in the experiment by Yokoo et al. [8]. Two configurations with the injector located at the bottom or side of the combustor were considered. The effects of injection from the combustor side wall on the flow field and thrust performance were investigated.

2 Numerical Aspects

The governing equations were three-dimensional compressible Euler equation and conservation low of 9 species (H_2, O_2, H, O, OH, H_2O, HO_2, H_2O_2, N_2). Also, to enclose the system, the equation of state was used assuming thermally perfect gas condition. ρ is density, p is pressure, e is total energy, R is gas constant, and T is temperature. The Subscript i shows the physical quantity for ith species.

$$\frac{\partial \mathbf{Q}}{\partial t}+\frac{\partial \mathbf{E}}{\partial x}+\frac{\partial \mathbf{F}}{\partial y}+\frac{\partial \mathbf{G}}{\partial z}=\mathbf{S}$$

$$\mathbf{Q}=\begin{bmatrix}\rho\\ \rho u\\ \rho v\\ \rho w\\ e\\ \rho_i\end{bmatrix},\mathbf{E}=\begin{bmatrix}\rho u\\ p+\rho u^2\\ \rho uv\\ \rho uw\\ (e+p)u\\ \rho_i u\end{bmatrix},\mathbf{F}=\begin{bmatrix}\rho v\\ \rho uv\\ p+\rho v^2\\ \rho vw\\ (e+p)v\\ \rho_i v\end{bmatrix},\mathbf{G}=\begin{bmatrix}\rho w\\ \rho uw\\ \rho vw\\ p+\rho w^2\\ (e+p)w\\ \rho_i w\end{bmatrix},\mathbf{S}=\begin{bmatrix}0\\ 0\\ 0\\ 0\\ 0\\ \omega_i\end{bmatrix}$$

$$p=\sum_i \rho_i R_i T$$

Thermodynamic properties were calculated by NASA polynomials [9]. The convective term is discretized by AUSM-DV [10] 3rd ordered by MUSCL method. Time integration method for fluid is 3 step 3rd order TVD Runge-Kutta method [11], and courant number is 0.3. Time integration for source term is Point implicit method with 5 times inner iteration. The chemical reaction model is that proposed by Hong et al. [12], which considers 20 elementary reactions including 9 species.

Figure 1 shows the calculation domain in this research. Two types of injector configurations, (a) the base injection and (b) the side injection, were considered. In reference to the short combustor in the experiment by Yokoo et al. [8], the combustor was set to 20 mm in length and diameter, and 24 injector pairs were arranged in the circumferential direction. The diameter of each injector is 1.2 mm. In addition, to simulate the flow field with the non-premixed inflow, two rows of injectors were arranged so that the unburned mixture collided with each other at 90°, as shown in Fig. 1(c). The center of the injector located at r = 8.5 mm and 6.5 mm for the base injection, at z = 2.0 mm and 4.0 mm for the side injection. In this analysis, the annular and orthogonal grids were overlapped, and the values were interpolated in r-θ plane. The number of grid points of annular region in the θ, r, and z directions was 1001 × 97 × 398 = 38.6 Mpts., and that of orthogonal region was 311 × 311 × 398 = 38.5 Mpts.. The grid width is 25.1-66.7 μm. The wall boundary is slip wall, and constant pressure of 10 kPa is set for outer region.

At the injector surface, the inlet conditions were changed dynamically depending on the pressure in the combustor, where the total pressure and total temperature were set to 1 MPa and 298.15 K. $2H_2$-O_2-$3.76N_2$ premixed gas was injected. When flow is choked, pressure is 0.528 MPa and temperature is

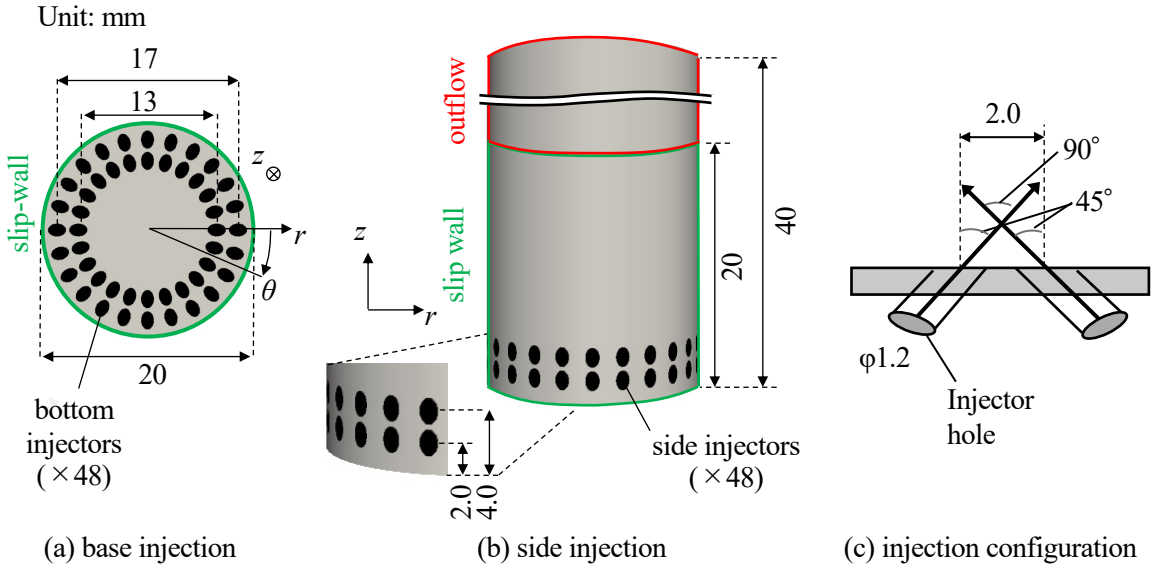

Figure 1: Calculation domain and condition. Injector configuration of (a) base injection, (b) side injection, and (c) injection configuration

248.4 K. In this condition, the induction length is 201.9 μm and the C-J velocity is 2012 m/s.

3 Result and Discussion

Figures 2 and 3 show the instantaneous pressure and temperature distribution in the combustor of the base injection and the side injection respectively. These figures show the pressure at r = 10 mm and the pressure and temperature at z = 3.5 mm. In addition, Table 1 shows the propagation velocities of the last 2 laps and thrust performance averaged during the last lap. D_{CJ} is for choked inflow condition.

Figure 2 shows the flow features of the base injection, which is the typical injector configuration. In Fig. 2 (a), there is one wave with large pressure increase, which propagates to the left direction in the figure. In Fig. 2 (b), there is a high-pressure region along the outer wall. This is corresponded to the propagating wave. The compression waves from the high-pressure region spread and gradually weakened as away from the detonation wave. This trend is similar to the numerical research by Tang et al. [7]. The temperature distribution in Fig. 2 (c) shows the low temperature unburned mixture in front of the wave and the high temperature gas behind the wave. The average propagation velocity of the last two laps was 2060 ms^{-1}.

Next, the characteristics of the flow field obtained in the side injection are described, in which the injectors are placed on the side of the combustor. Figure 3 (a) shows two vertical thin waves and high-pressure regions near the injector. These waves propagated to the left in the combustor like the wave in base injection. In Fig. 3 (b), the high-pressure regions corresponding the propagating waves are observed, and pressure is high in a wide range of the combustor. In the temperature distribution in Fig. 3 (c), there is low temperature unburned mixtures near the outer wall from the side injectors. The burned gas is observed near the center of the combustor. The average propagation velocity of the last two laps was 1442 ms^{-1}. Thus, there was difference in the flow field in the combustor depending on the injector configuration.

To compare the differences in the flow field obtained for different injector configuration, Fig. 4 (a) (b) shows the axial pressure profiles in the combustor, (a) the instantaneous maximum pressure and (b) the spatiotemporal average pressure to the distance from the bottom z. The maximum pressure profiles are in the same moment as in Figs. 2 and 3, and the average pressure profiles are averaged during the last

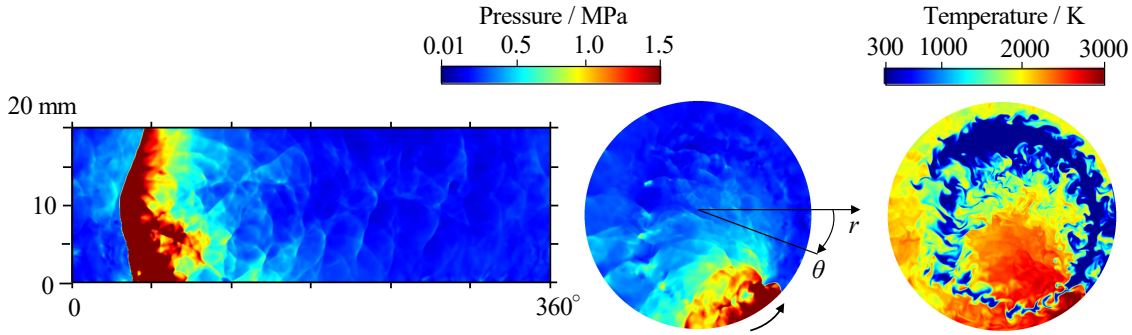

(a) Pressure (r = 10 mm, outer wall) (b) Pressure (z = 3.5 mm) (c) Temperature (z = 3.5 mm)

Figure 2: Flow fields in the base injection case. (a) pressure (r = 10 mm, outer wall), (b) pressure (z = 3.5 mm), and (c) temperature (z = 3.5 mm).

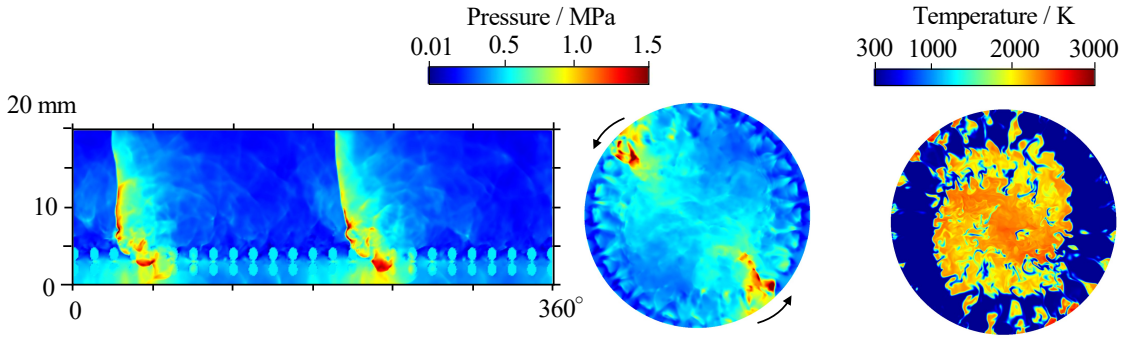

(a) Pressure (r = 10 mm, outer wall) (b) Pressure (z = 3.5 mm) (c) Temperature (z = 3.5 mm)

Figure 3: Flow fields in the side injection case. (a) pressure (r = 10 mm, outer wall), (b) pressure (z = 3.5 mm), and (c) temperature (z = 3.5 mm).

lap. In the instantaneous maximum pressure profiles, the pressure of the base injection is especially high under the z = 10 mm. For the averaged pressure profiles, a similar profile is obtained from z = 5 mm to the outlet. Below z = 5 mm, the averaged pressure of the side injection is higher than that of the base injection, with a maximum difference of about 30%. In summary, the maximum pressure was particularly high for the base injection, which has a high propagation velocity, but when averaged, similar pressures were obtained for both injector configurations.

Figure 4 (c) (d) shows the spatiotemporal average profiles of (c) the mole fraction of H_2 and (d) the axial Mach number during the last lap. Figure 4 (c) shows different peaks depending on the injector configuration, with a maximum at the bottom for the base injection and at around z = 3.5 mm for the side injection. This is due to the difference of z-position of the injectors. However, the fuel consumed to the combustor outlet under both conditions. At the combustor outlet, the mole fraction of H_2 in the base injection is larger by 0.0113 than that in the side injection. In Fig. 4 (d), the axial Mach number of the base injection was particularly large near the bottom. Although the Mach number near the bottom is small in the side injection, acceleration of the burned gas was obtained to the combustor outlet as well. In both cases, the burned gas was accelerated to about the speed of sound.

Finally, the thrust and specific impulse are shown in Table 1 with theoretical values. The thrusts in this simulation are averaged during one lap propagation. These values are calculated as the summation of the momentum and pressure thrusts with the control surface method [13]. The theoretical values are calculated using the values from NASA-CEA [14] assuming constant-pressure combustion, frozen flow, and sonic exhaust. From Table 1, the specific impulse was 176 s for the base injection and 164 s for the

Table 1: Summary of the results of mass flow rate, propagation velocity, and thrust performance

Injector configuration	$\dot{m}$ / gs^{-1}	D / ms^{-1}				Thrust / N		I_{sp} / s	
		D_1	D_2	D_{ave}	D_{CJ}*	F	F_{theory}	I_{sp}	$I_{sp,theory}$
base	99.1	2009	2111	2060	2012	171	167	176	172
side	100	1468	1416	1442		162	168	164	172

* choked inflow condition

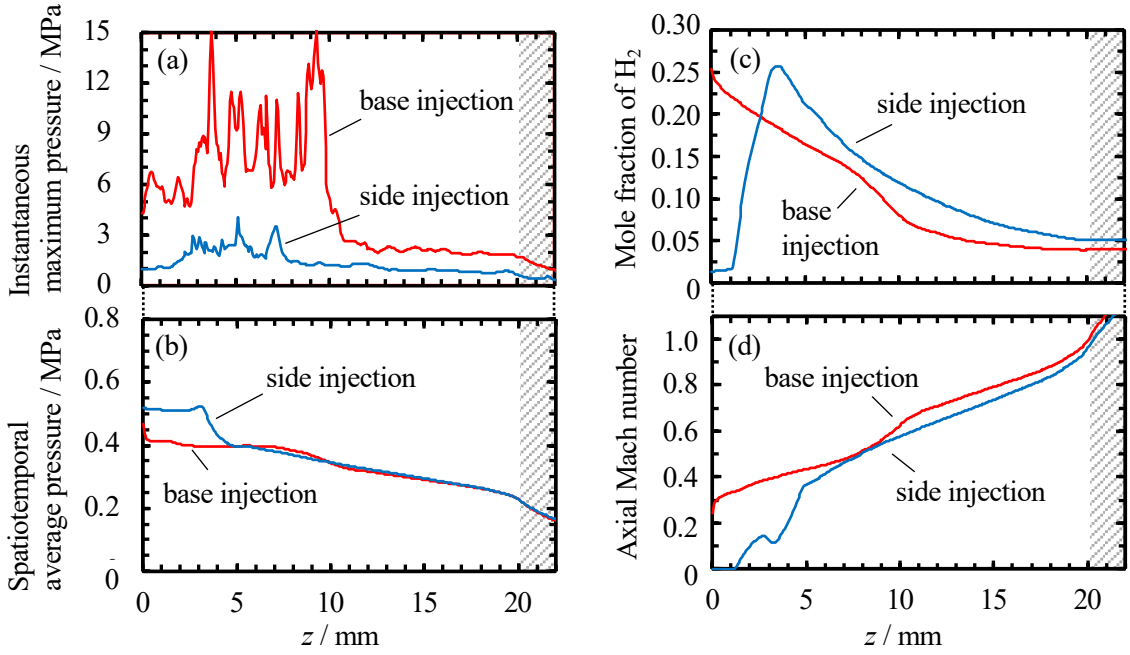

Figure 4: Axial profiles. (a) instantaneous maximum pressure, (b) spatiotemporal average pressure, (c) spatiotemporal average mole fraction of H_2, and spatiotemporal average axial Mach number.

side injection, which was 102.3 % and 95.4 % of the theoretical value. This result shows that it is slightly inferior to the theoretical specific impulse in the side injection, but the performance is close. This could be due to differences in the amount of fuel consumption over the combustor outlet.

4 Conclusion

We have numerically investigated the cylindrical RDE combustor with 20 mm in diameter and length using the stoichiometric hydrogen-air premixed gas. Two types of the injector configurations, the base injection and the side injection, were examined. The following findings are obtained.

From the pressure fields and profiles, the shape of the propagating waves varied depending on the injector configuration. In the side injection, the thin waves and high-pressure near the injector are observed. In addition, the average mole fraction profile of H_2 in r-θ plane indicates that H_2 is consumed to the combustor outlet in both cases, and the burned mixture accelerates to sonic flow toward the outlet. The specific impulse of the side injection case was 95.4% of the theoretical value. There were differences in wave structure depending on the position of the injector, but the effect on the performance of the short combustor is small. Thus, we concluded that in the short cylindrical combustor, RDE with injectors on the combustor side wall, which was proposed to reduce the heat load of the combustor wall in the previous research, can provide similar performance with the injection from the bottom.

Acknowledgments

This study was financially supported by JSPS KAKENHI Grants No. JP19H05464 and by the Institute of Space and Astronautical Science of the Japan Aerospace Exploration Agency. Part of the numerical results were obtained using supercomputing resources at Cyberscience Center, Tohoku University.

References

[1] Y.B.Zel'dovich, "To the Question of Energy Use of Detonation Combustion", Journal of Propulsion and Power, Vol. 22, No. 3, pp. 588-592, 2006 (Translation of Article Originally Published in Russian in Zhurnal Tekhnicheskoi Fiziki, 10, pp. 1453-1461,1940.

[2] P. Wolanski, "Detonative Propulsion", Proceeding of the Combustion Institute, 34, pp. 125-158, 2013.

[3] F. A. Bykovskii, and E. F. Vedernikov, "Heat Fluxes to Combustor Walls during Continuous Spin Detonation of Fuel-Air Mixtures", Combustion, Explosion, and Shock Waves, 45 (1), pp. 70-77, 2009.

[4] J. Braun, J. Sousa, G. Paniagua, Numerical Assessment of the Convective Heat Transfer in Rotating Detonation Combustors Using a Reduced- Order Model, Applied Science, 8, 893-907, 2018.

[5] K. Goto, K. Ota, A. Kawasaki, N. Itouyama, H. Watanabe, K. Matsuoka, J. Kasahara, A. Matsuo, and I. Funaki, H. Kawashima, "Cylindrical Rotating Detonation Engine with Propellant Injection Cooling", Journal of Propulsion and Power, 2021.

[6] R. Yokoo, K. Goto, J. Kim, A. Kawasaki, K. Matsuoka, J. Kasahara, A. Matsuo, and I. Funaki, "Propulsion Performance of Cylindrical Rotating Detonation Engine", AIAA Journal, 58(12), 2020.

[7] X. M. Tang, J. P. Wang, and Y. T. Shao, "Three-dimensional numerical investigations of the rotating detonation engine with a hollow combustor", Combustion and Flame, 16, pp. 997-1008 2015.

[8] R. Yokoo, K. Goto, J. Kasahara, V. Athmanathan, J. Braun, G. Paniagua, T. R. Meyer, A. Kawasaki, K. Matsuoka, A. Matsuo, I. Funaki, "Experimental study of internal flow structures in cylindrical rotating detonation engines", Proceeding of the Combustion Institute, 38 (3), pp. 3759-3768, 2021.

[9] B. J. McBride, S. Gordon, M. A. Reno, "Coefficients for Calculating Thermodynamic and Transport Properties of Individual Species", Nasa Technical Memorandum, 4513, 1993.

[10] Y. Wada, M. Liou, "An Accurate and Robust Flux Splitting Scheme for Shock and Contact Discontinuities", Journal of Scientific Computing, 18 (3), pp. 633-57, 1997.

[11] S. Gottlieb, S. Chi-wang, "Total Variation Diminishing Runge-Kutta Schemes", Mathematics of Computation, 67, pp. 73-85, 1998.

[12] Z. Hong, D. F. Davidson, R. K. Hanson, "An improved H2/O2 mechanism based on recent shock tube/laser absorption measurements", Combustion and Flame, 158, pp. 633-644, 2011.

[13] J. E. Shepherd, J. Kasahara, "Analytical Models for the Thrust of a Rotating Detonation Engine, Caltech GALCITFM, California Institute of Technology", Pasadena, CA, 2017.

[14] S. Gordon, B. J. McBride, "Computer Program for Calculation of Complex Chemical Equilibrium Compositions and Applications", NASA Reference Publication 1311 1994.